Arctic sea ice and snow from different ice models: A CICE–SI3 intercomparison study

Imke Sievers[1,3], Andrea M. U. Gierisch[1], Till A. S. Rasmussen[1], Robinson Hordoir[4,5], and Lars Stenseng[2]

[1]Danish Meteorological Institut, Lyngbyvej 100, Copenhagen East, Denmark
[2]DTU Space, Danish Technical University, Elektrovej Bygning 327, 2800 Kongens Lyngby, Denmark
[3]Aalborg University,A. C. Meyers Vænge 15, 2450 Copenhagen, Denmark
[4]Institute of Marine Research, Bergen, Norway
[5]Bjerknes Centre for Climate Research, Bergen, Norway

Correspondence: Imke Sievers (imksie@dmi.dk)

Abstract. Sea-ice models fill many purposes; they are used in global climate models or for short-term forecasts to plan shipping routes. No matter what their output is used for, understanding the cause for their variability is crucial.

In the this study two commonly used sea-ice models, CICE and SI3 were compared after running both models with similar boundary condition, on the same grid, with the same forcing and initialised with the same data, with the aim to understand how

5 the two models differ from each other when forced equally. The set-up also allows linking certain model biases observed in both models to the external forcing. We found that the models compare well to sea ice concentration, sea ice thickness and snow thickness observations, with small regional differences, which could be linked to different model processes. The processes with the highest influence are the drag formulation, the albedo, and the treatment of snow. We find that the treatment of snow has a significant influence on the difference in sea ice thickness between the models, even though their forcing is equal.

1 Introduction

10 The interest in forecasts of Arctic sea ice conditions on multiple time scales has increased. On short time scales (up to days) forecasts are of importance for search and rescue and maritime safety (Wagner et al., 2020). As the forecast length is extended towards seasonal the variability in the Arctic sea ice cover is of interest when planning shipping routes and other maritime activities (Stocker et al., 2020; Stewart et al., 2020). On long time scales (decades and more) forecast of the Arctic sea ice cover are of interest for the climate science community as it plays a central role in the global climate system as changes in

15 the sea ice cover changes the albedo of the poles and thereby provides a positive feedback to the climate system (Kashiwase et al., 2017). Validation of model systems are primarily based on remotely sensed data as in-situ data is difficult to obtain in the Arctic. Long records of sea ice concentration (SIC) are often based on remotely sensed passive microwave data, which extends back to the 1970s. In addition to validation, these data sets provide time series of the historical evolution of the sea ice cover.

20 Within this time period sea ice extend has retreated and the fraction of multi-year sea ice has reduced (Tonboe et al., 2016). Hindcast from sea-ice models aim to reproduce and predict these changes. One example is Collow et al. (2015), who show

the same trend for sea ice volume as what is seen in the remotely sensed data records. However, two model simulations rarely result in the exact same result.

Several studies have examined the cause of these differences. The influencing parameters can in general be grouped into external and internal parameters. External parameters are for example atmospheric forcing, lateral boundary conditions or initial conditions. Atmospheric forcing for example influences sea ice by adding heat, precipitation and radiation. Wang et al. (2018) compared the widely used atmospheric reanalysis ERA-Interim with its successor ERA5, which has on average a 2° C higher warm bias. Forcing a 1-D thermodynamic model with both dataset resulted in an unexpected low difference since ERA5s precipitation is higher and insulated the sea ice from heat loss. Another example of an external parameter for differences are the initial conditions. They are especially interesting for short-term predictions. When cold starting a model run the initial SIC and thickness are often depending on the ocean and atmosphere temperature and are constant. To avoid over or underestimated ice they are often set to a value realistic in the area of interest. Dirkson et al. (2017) and Day et al. (2014) run simulations where observed SIC and thickness were used as initial conditions and show that the skill of the model increases significantly when a realistic sea ice thickness (SIT) is used.

Internal parameters are for example the model grid, time steps, number of sea ice categories or the way thermodynamic and dynamic processes are discretized. Kiss et al. (2020) compares three global ocean-sea-ice models on three different fine grid resolutions and finds that different resolutions favour the representation of different process. They for example find that models run on coarser girds miss certain sea ice characteristic features as for example leads. Another example of internal cause for resulting model differences is the dynamical solver chosen to solve the momentum equation of sea ice. Losch et al. (2010) compares a line-successive-over-relaxation (LSOR) an a elastic-viscous-plastic (EVP) scheme finding that the resulting sea ice velocities differ by several cm/s resulting in a freshwater export difference of 200 km^3 yr^{-1}.

Many solutions as, for example the dynamical solver, the grid size, and the number of sea ice categories increase the computational cost. Many sea-ice models, which are commonly used, come with a limited set of options for internal parameters as for example the dynamical solver, or the way albedo is calculated from the radiative forcing. This leads to many different sea-ice model set ups, which when compared to one another still show to have comparable skill (Long et al., 2021), however they still show a certain amount of variability in Arctic sea ice conditions. In order to set up an ideal sea-ice model, the external and the internal parameters and forcing should reflect the reality, as close as possible, however it can be hard to differentiate the sources that introduces the bias between the external and internal parameters. In order to study the internal parameters only the external forcing can be set to be the same.

In this study, we want to investigate this variability. This is done by using two state of the art sea-ice models which are commonly used to simulate Arctic sea ice at different time scales such as climate models (Long et al., 2021), short term sea ice predictions (Dupont et al., 2015) and in sea ice reanalysis (Lellouche et al., 2021). In order to focus the analysis on the sea-ice models the two models were run on the same grid, with the same atmospheric forcing, coupled to the same ocean model, forced by the same boundary conditions and started from the same ocean and sea ice initial conditions to eliminate sources influencing the sea ice predictability. The models are CICE and SI3. SI3 is the default sea-ice model included in NEMO after version 4.0.

Since CICE can be run stand-alone or coupled to an ocean model, CICE was coupled to NEMO. To our knowledge this study is the first coupling NEMO4 to CICE and this study also serves as a validation study.

Snow plays an important role in the sea ice thermodynamics as it acts as an insulating layer between the atmosphere and the sea ice. It has a high albedo which ensures that the incoming radiation is reflected. It also plays a part in sea ice dynamic
60   processes as it alters the surface roughness of sea ice. During the last year snow on sea ice gained more and more attention. New satellite based snow observation data products were released as for example the Ka/Ku band snow product from LEOGS (Garnier et al., 2021) or the snow depth resulting from a combination of Cryosat2 and ICESat2 sea ice freeboards by Kacimi and Kwok (2022). The increased understanding has also reached the modelling community with the result that snow becomes more and more important (Blanchard-Wrigglesworth et al., 2015). For these reasons we decided to include the snow volume
65   in this study to contribute to the understanding which role snow plays in sea ice models.

The aim of this study is to compare the two models under as similar conditions as possible and investigate the significant differences which may appear. In addition, if there are significant differences we want to identify and discuss their causes. Based on this we want to make a statement about where the sea-ice modelling community might need to put a focus for further improvement.

70   Section two describes the data, methods including the models used in this study. Section three describes the results and highligths the differences between the two ice models, whereas section four discuss the results and section five concludes this study.

2   Data and Models

The two coupled ocean and sea ice model systems consist of the same ocean model, which is described in section 2.1, and
75   two different sea ice models, which are introduced in section 2.2, together with their setup and input data. In section 2.3 the observational data which was used for the evaluation is described.

2.1   Ocean model

The ocean model NEMO (Madec et al., 2017) is widely used in the modelling community for both regional (Le Sommer et al., 2019) and global ocean simulations, climate prediction, hind casts (Hazeleger et al., 2012) and modelling of marginal seas
80   (Hordoir et al., 2019) to only name a few applications. The set up used in this paper closely follows Hordoir et al. (2022) and uses similar forcing and namelist settings. Changes were made to the namelist due to a version update and the atmospheric forcing differs. The setup includes tides and runs without ocean surface restoring. The forcing consists of 3-hourly atmospheric data from ERA5 (Hersbach et al., 2017) (2-m temperature, 2-m specific humidity, 10-m wind, incoming short/long wave radiation, total precipitation, snowfall and sea level pressure). At the lateral boundaries it is forced monthly with GLORYS
85   salinity, temperature, u- and v-velocities and sea surface height fields (Lellouche et al., 2021). The tidal forcing consists of TPXO 7.2 harmonic tidal constituents at open boundaries (Egbert and Erofeeva, 2002). For the river runoff a climatology from

Dai and Trenberth (2002) was used. The initial fields for salinity, temperature, SIC and SIT for ocean and ice are ORAS5 reanalysis (Zuo et al., 2019).
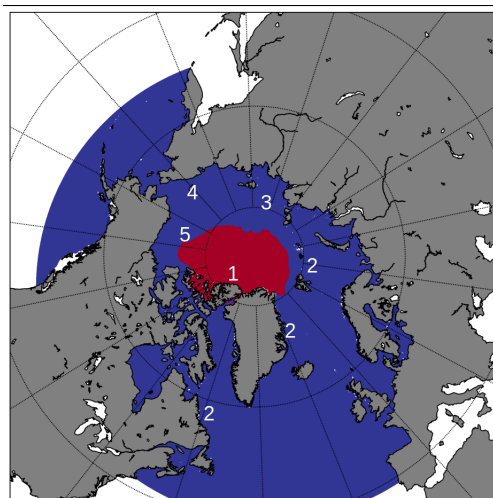
Figure 1. The model domain of the coupled NEMO-CICE and NEMO-SI3 models (area in blue and red). The red area refers to the thick ice mask used in figure 9 and the blue area to the thin ice mask used in figure 9. The thin ice mask also includes open water and its southern borders mark the end of the model domain. The numbers indicate different areas discussed in section 4. Number 1 indicates the Lincoln Sea and Canadian Archipelago, 2 the Atlantic ice edge, 3 the Russian shelf, 4 the Chukchi Sea and 5 the Beaufort sea.

2.2 Sea ice models

90 Both sea-ice models are coupled to NEMO. The sea-ice models CICE (Hunke et al., 2021a) and SI3 (NEMO-Sea-Ice-Working-Group, 2022) both are eulerian multi category sea-ice models solving dynamics, and thermodynamics of sea ice numerically. Both models use Elastic-Viscous-Plastic (EVP) rheology run with the same time step, and are coupled and forced at the same frequency. The models were run from 2008 to 2020 starting from the same initial conditions. The model output analysed in the following sections includes data from 2010-2020, excluding a 2 year spin up phase. The albedo was tuned in both models.

95 Since the calculation of the albedo differs in both models this could not be made coherently. The tuned parameters are attached in the supplementary material along with their models namelists.

2.2.1 SI3

SI3 (Sea-Ice Integrated Initiative) is the NEMO default sea-ice model from version 4.0. It was developed to unify the former three main sea-ice models used in combination with NEMO in the past: CICE, GELATO and LIM (Madec et al., 2017). SI3 uses

100 constant drag coefficients for ocean ice and atmosphere ice drag. The parameters can be found in the namelist in the appendix. The albedo calculation follows (Shine and Henderson-Sellers, 1985) and distinguishes in between five different surface types which which all can be tuned via namelist parameters, which can be found in the appendix. The albedo parameters were tuned

to fit the Pan-Arctic Ice Ocean Modeling and Assimilation System (PIOMAS) (Schweiger et al., 2011a) total sea ice volume. For this study we use NEMO-SI3 version 4.0.4 revision r13658.

2.2.2 CICE

CICE is a portable sea-ice model, which can be used standalone, however it is recommended to run as part of a coupled system either global or regional. The model consists of one dynamical part solving advection of sea ice and changes in thickness and a thermodynamic model solving the changes in thickness due to thermodynamic processes. The code for both parts is frequently updated and maintained by the CICE consortium and can be found on github (Hunke et al., 2021a).

In this set up we use form drag formulation which calculates the drag coefficients depending on SIC, flow size, melt pond, ridges and freeboard as described by Tsamados et al. (2015). The albedo is calculated depending on the suns incident angle and sea ice surface type following Briegleb and Light (2007). The different surfaces types are snow, ice and melt ponds. For the calculation of the surface albedo different process are taken into account. For a more detailed description we refer to Hunke et al. (2021b). The albedo parameters were tuned to fit PIOMAS (Schweiger et al., 2011a) total sea ice volume.

CICE is coupled to NEMO based on a set up used in Smith et al. (2021). Changes made from Smith et al. (2021) to the present setup are the update of the model versions from NEMOv3.6 to NEMOv4 and CICEv4 to CICEv6.2. As a difference to the standard setting the freezing and the melt temperature has been differentiated in order to account for salinity difference of sea ice and the ocean.

2.3 Observations

The model simulations are compared with remote sensing observations of SIC, SIT and snow depth on sea ice. Therefore monthly averages of model output were interpolated to the observation grids. All averages were calculated over the period 2010-2020.

2.3.1 OSISAF Sea ice concentration

The Ocean and Sea Ice Satellite Application Facility (OSISAF) SIC is based on passive microwave data from satellite measurements. Brightness temperature measurements retrieved by SSMIS instruments are processed with help of ECMWF atmospheric reanalyses on a daily basis by DMI and MET Norway. The advantage of using brightness temperatures to retrieve SIC is the independence of cloud cover and daylight in the Arctic, resulting in a year round data product. The data is gridded in a resolution of 10x10km covering the entire Arctic. It has an accuracy of ± 10% in the Arctic with the largest bias in summer due to meltponds (OSISAF, 2017).

2.3.2 CS2SMOS Sea Ice Thickness

The CS2SMOS SIT product is an optimal interpolated sea ice product combining weekly averaged CryoSat2 SIT with daily SMOS SIT developed by the Alfred Wegener Institue (AWI). The combination of these two products utilise their combined

strength; the thick sea ice from Cryosat and the thin sea ice from SMOS (Mu et al., 2018b). Data comes on a 25x25km EASE2 grid with a time step of one week. More information about the data set can be found in Ricker et al. (2017).

2.3.3 Ka/Ku Snow Thickness

The Ka/Ku snow depth product combines altimeter data from SARAL and from CryoSat2. It uses the difference in penetration depths from Ka-band and Ku-band altimeters to determine how much snow lays on top of sea ice. This is possible because the Ku-band radar is reflected at the snow–ice interface, while the Ka-band radar is reflected at the snow surface. The data product comes in monthly time steps covering the time period November to April 2013-2019. The data is distributed on a 12.5km x 12.5km EASE2 grid and covers the Arctic up to 81.5N (Garnier et al., 2021).

3   Results

This section will describe comparisons of the two model systems and SIC, SIT and snow thickness with each other and with observations.

3.1   Sea Ice Concentration

Figure 2 shows the 10 year mean OSISAF SIC compared to 10 year mean modelled SIC for March and September. In general, the differences are slightly larger in CICE compared to SI3, but this difference is small in comparison to the model-observation differences. In March, the largest differences are found in the North Atlantic and Barent Sea. In September, both models show a higher SIC in the Beaufort Sea and a lower SIC in the central Arctic close to the Russian shelf. The negative bias of the models in the Beaufort Sea is stronger pronounced in CICE. The positive bias in SI3 in the Central Arctic/Russian shelf region is stronger pronounced in SI3.

Figure 3 shows the difference between SI3 and CICE and the SIC for the respective month September and March. In March, the differences are mainly in the Atlantic sector with more SIC in CICE. At the maximum CICE exceeds SI3 SIC by 60% just north of Iceland. In average CICEs SIC exceeds SI3s by about 25% in the region where the models differ from each other. In September, CICEs SIC is larger than SI3s close to the ice edge. Here the maximum of this difference lies with 50% more SIC in CICE compared to SI3 in the northern Laptev Sea. The central Arctic and the area north of Greenland SI3 has up to 20% higher SIC than CICE.

3.2   Sea Ice Thickness

To compare the models with the CS2SMOS all the monthly SIT model data was interpolated onto the CS2SMOS grid. Only data points covered by CS2SMOS were considered for the comparison and all data above 88° N was excluded, since CS2SMOS is an optimal interpolation and not CryoSat2 nor SMOS covers latitudes above 88° N. Data from each month in which CS2SMOS is available was summed up over the total covered area and is shown for both models and CS2SMOS in figure 4.
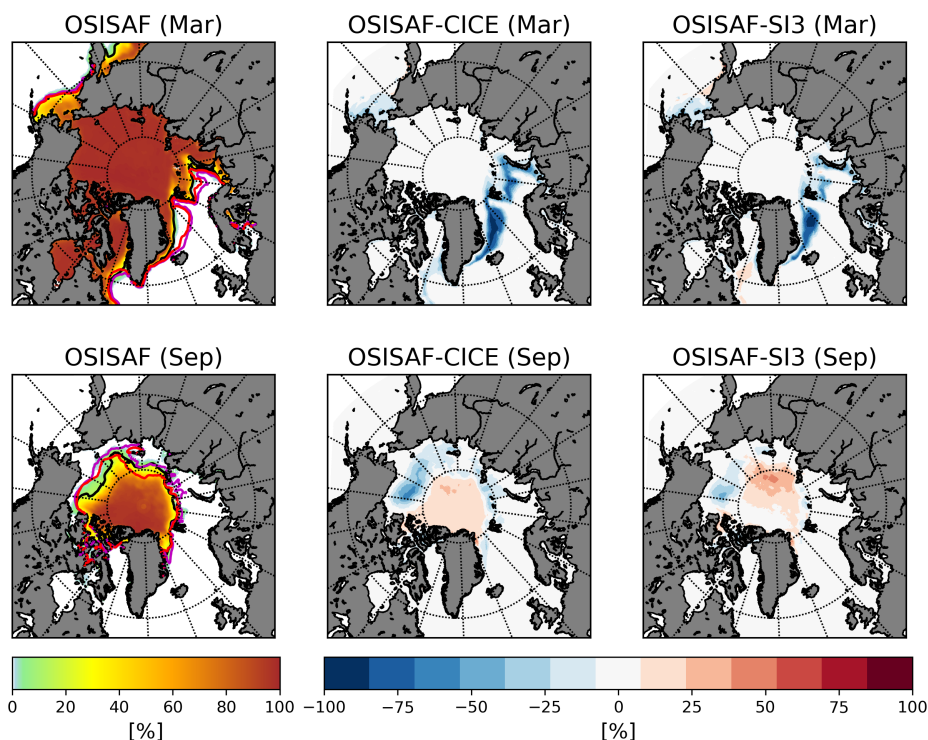
Figure 2. Monthly SIC climatology and differences for the period 2010-2020. March is shown in the upper row and September in the lower row. Left panel displays OSISAF observation, the middle the difference of OSISAF and CICE and on the right OSISAF minus SI3. The black line shows the 15% SIC contour from OSISAF, the red line from SI3 and the purple line from CICE for the respective month.

3.2.1 Model Satellite Comparison

Figure 4 shows that in most years CS2SMOS starts the winter season with a larger sea ice volume compared to the models. In most years, when the freeze up begins CICE models the sea ice cover to be thinner than the ice cover from SI3. Throughout

165 the rest of the winter season, the modeled sea ice volume grows faster compared to the CS2SMOS sea ice volume. While CS2SOMS stop increasing the sea ice volume in April, both models keep on producing sea ice until the end of the season. CICE slows down the sea ice production slightly earlier than SI3. This is especially true from 2012 to 2016.

To get a better understanding of the regional differences between models and observations monthly difference maps of 10 year averages for October and March are plotted along with a reference CS2SMOS SIT in figure 5. The figure shows that the

170 overall lower sea ice volume in October, also shown in figure 4 originates from a difference in the central Arctic. Overall, this difference is stronger between CICE and CS2SMOS than between SI3 and CS2SMOS. In March, both models show a thicker ice cover than CS2SMOS in coastal areas (Canadian Archipelago, Hudson Bay, Russian shelf seas) and at the ice margins around western Greenland. The SIT differences in the central Arctic is approximately the same as in October. In the Beaufort Sea region, both models display more ice than CS2SMOS for all months. This difference is strongest pronounced
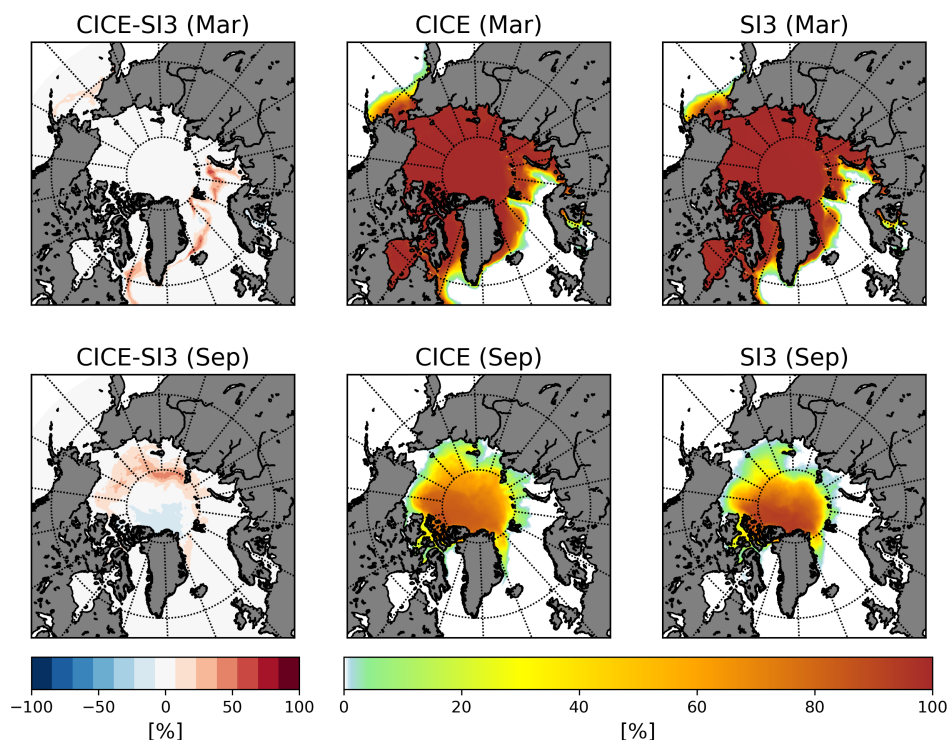
Figure 3. Monthly SIC climatology and differences for the period 2010-2020. First column shows the difference in SIC between the two model setups in March (top) and September (bottom) and the respective SIC for CICE and SI3 (second and third column) in 10 year monthly mean for March (upper row) and September (lower row).
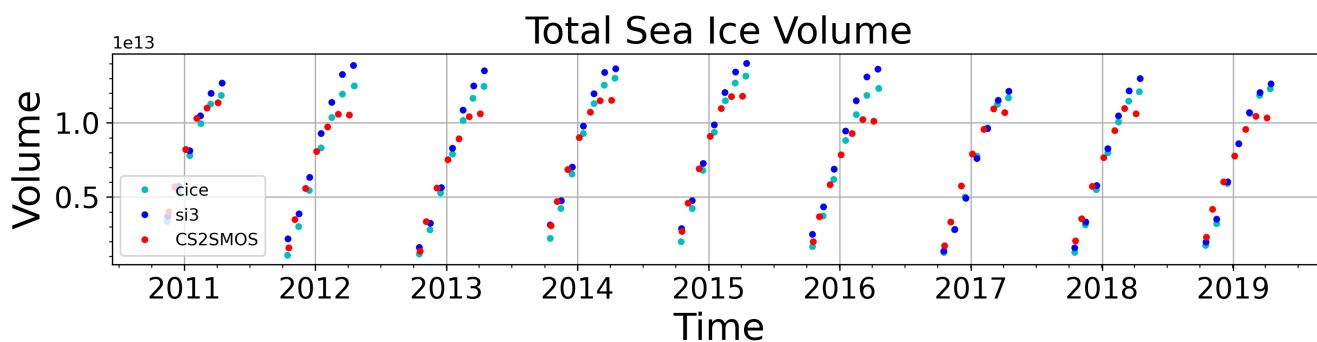
Figure 4. Sea ice volume variation of CICE (light blue), SI3 (dark blue) and CS2SMOS (red) for October - April 2010 to 2019

175 in SI3 compared to CICE. SI3 shows a thicker ice cover just north of Greenland for all months. In CICE, this area is in both March and October close to C2SMOS SIT. Both models display a more homogeneous SIT throughout the Arctic compared to
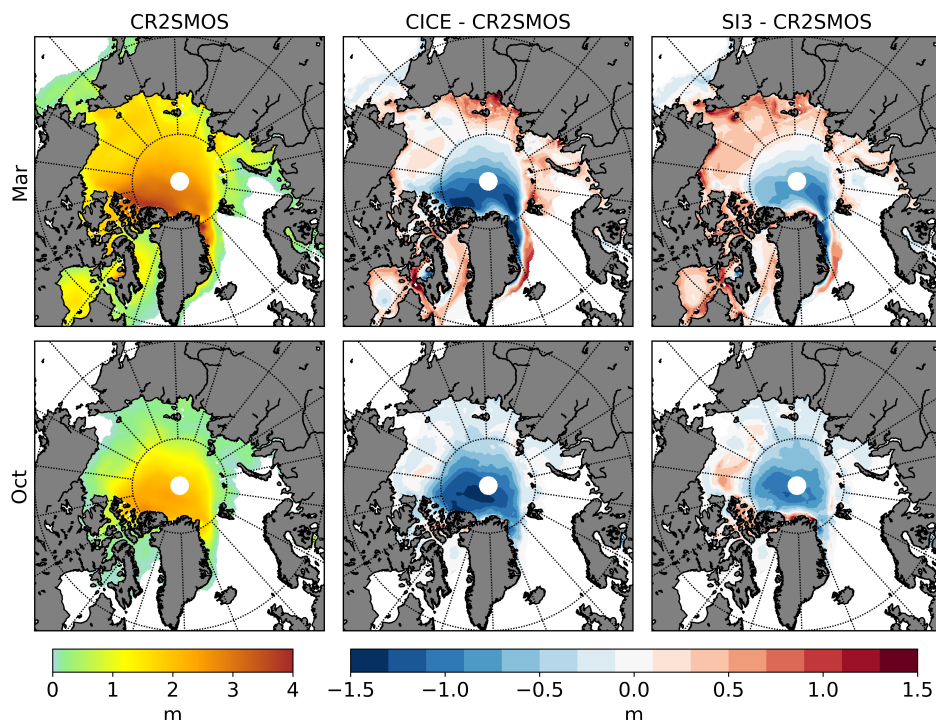
Figure 5. Monthly SIT climatology and differences for the period 2010-2020 for March and October. The left column shows CR2SMOS SIT the middle CICE-CR2SMOS and the right SI3-CR2SMOS.

observations with less thick ice in the central Arctic and thicker sea ice towards the margins. In general, the locations in which the models differ from CS2SMOS are similar.

Figure 6 compares the ice thickness of the two model systems. CICE SIT is in general thinner than the SI3 SIT in the regions north of Greenland and in the Beaufort Sea. In March, CICE SIT is over all thinner than SI3s SIT in most regions. This is shown in 6 upper left panel. Only close to the ice edge, in the Atlantic sector and in the Laptev Sea CICE sea ice is up to 0.7m thicker than SI3. SI3 is up 1m thicker than CICE in Chucki Sea, north of Greenland and the Canadian archipelago. In September SI3 SIT (lower left panel 6) is thicker in the region north of Greenland, the Canadian archipelago and the Beaufort sea and CICE is thicker than SI3 on the Russian shelf break.

3.3 Snow

Modeled and observed snow thickness distributions are shown in figure 7. The Ka/Ku data product only covers the Arctic up until 81.5° N, which excludes a larger part of the multiyear sea ice, see figure 1. To compare data sets, monthly model data was interpolated onto the Ka/Ku grid and all data points not covered by the satellite observations were excluded. The resulting monthly thickness distribution for the period 2013-2019 is shown in figure 7 as a probability density function (PDF). Both
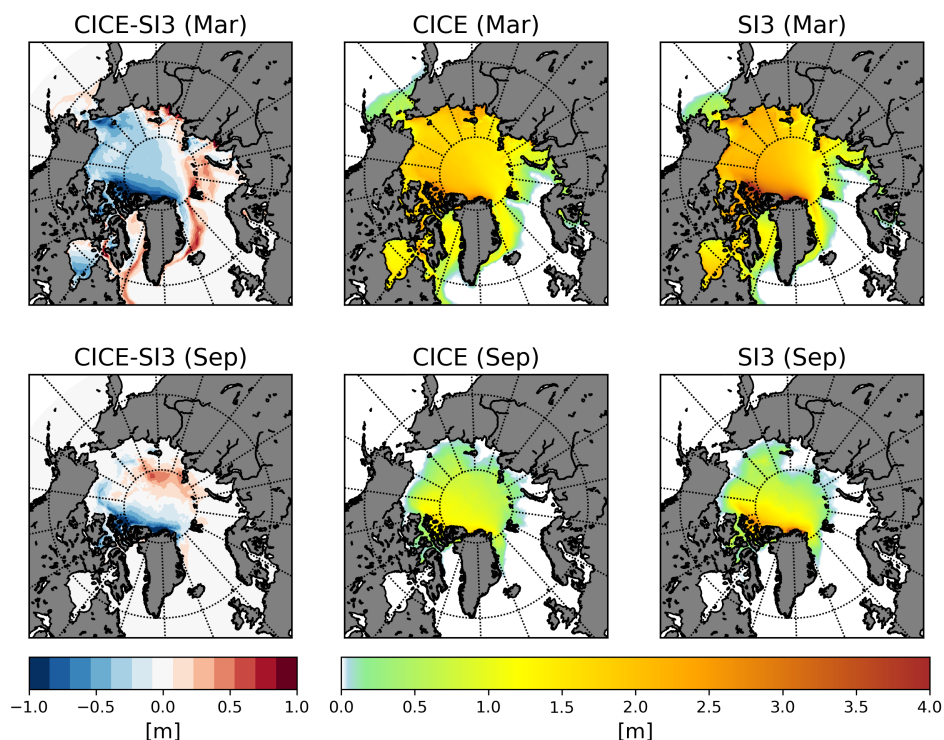
Figure 6. Arctic wide CICE and SI3 SIT comparisons for March (upper row) and September (lower row). The left panels show CICE-SI3 SIT, the middle CICE and the right SI3 SIT.
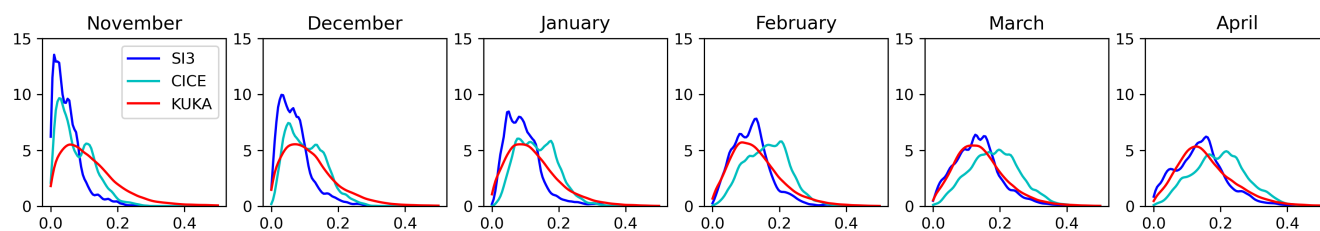
Figure 7. Pdfs of the snow thickness distribution for CICE (turquoise), SI3 (blue) and Ka/Ku (red) snow thicknesses. a) The pdf for the entire area covered by the Ka/Ku data product , b) for the Canadian Arctic marked as yellow in fig 1 and c) for the Russian Arctic marked as green in fig 1 for the month November, December, January, February, March and April. Note the different x-axis for a).

models have a limited snow cover which is only a few cm thick in November, whereas the snow thickness in the observations is around 10cm. The dominant snow thickness increases over the winter season in the models. In April, the dominant snow thickness in CICE is about 22cm and 18cm in SI3. The dominant snow thickness in the observations (red line) moves from approximately 8cm in November to about 15cm in April. CICE agrees more with the observed snow thickness distribution in

the beginning of the season, whereas SI3 agrees more with observations in the end of the season. Especially in March and April

195 SI3 shows good agreement with observations. Overall, the models show a more noisy distribution than the observations.
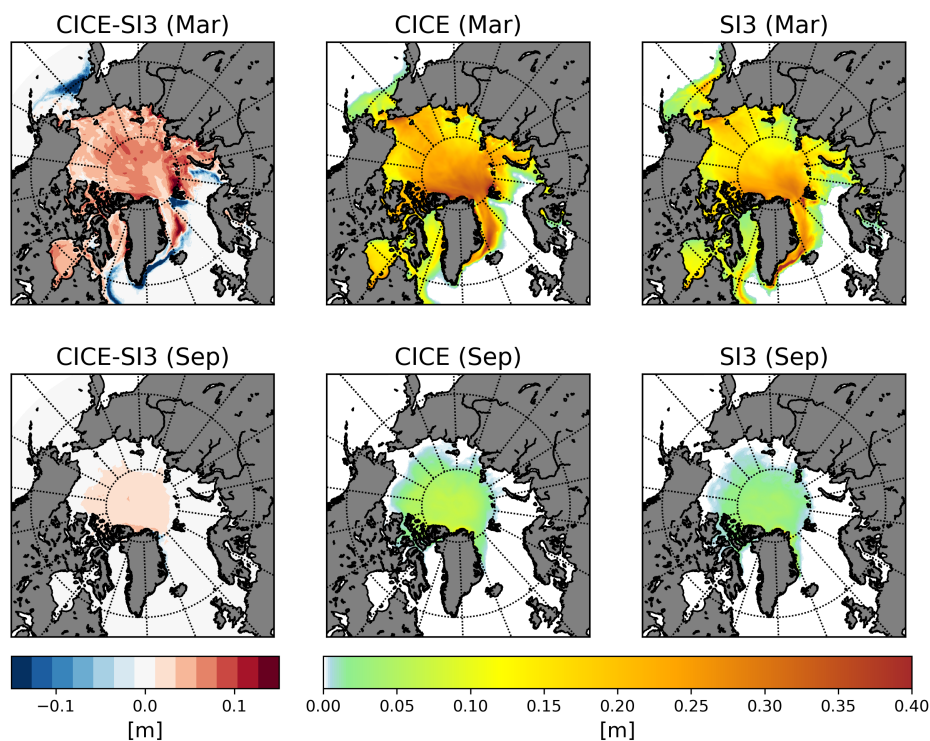
Figure 8. March (lower panel) and September (upper panel) monthly Arctic wide snow thickness climatologies calculated over the period 2010-2020. The left column shows the difference CICE-SI3 snow thickness the middle CICE and the right SI3 total snow thickness.

Figure 8 shows the snow cover of both models (CICE: middle, SI3: right) in March and September and their differences (left). In September, CICE has a 5cm snow cover in most of the central Arctic while SI3 only shows a few cm in small patches in the central Arctic and off the coast of north Greenland and the Canadian Archipelago. In March CICE and SI3 build up a snow cover of up to 40cm. In CICE, this maximum is located between Iceland, Greenland, and north of Svalbard. In SI3 the

200 maximum is located south west of Svalbard and along the ice edge southeast of Greenland. The difference map for March shows that overall CICE has a 8-10cm thicker snow cover than SI3 in almost the entire Arctic. Only close to the ice edge, SI3 has up to 15cm more ice than CICE.

3.4 Regional sea ice and snow volume comparison

Analyses of the modelled total sea ice volume and total snow volume development throughout the year show a seasonal and

205 regional difference between the models. This seasonality is shown in 9. The curves in 9 were calculated by subtracting CICE total Arctic sea ice and snow volume from SI3. Figure 9 upper panel shows the total Arctic snow volume and sea ice volume
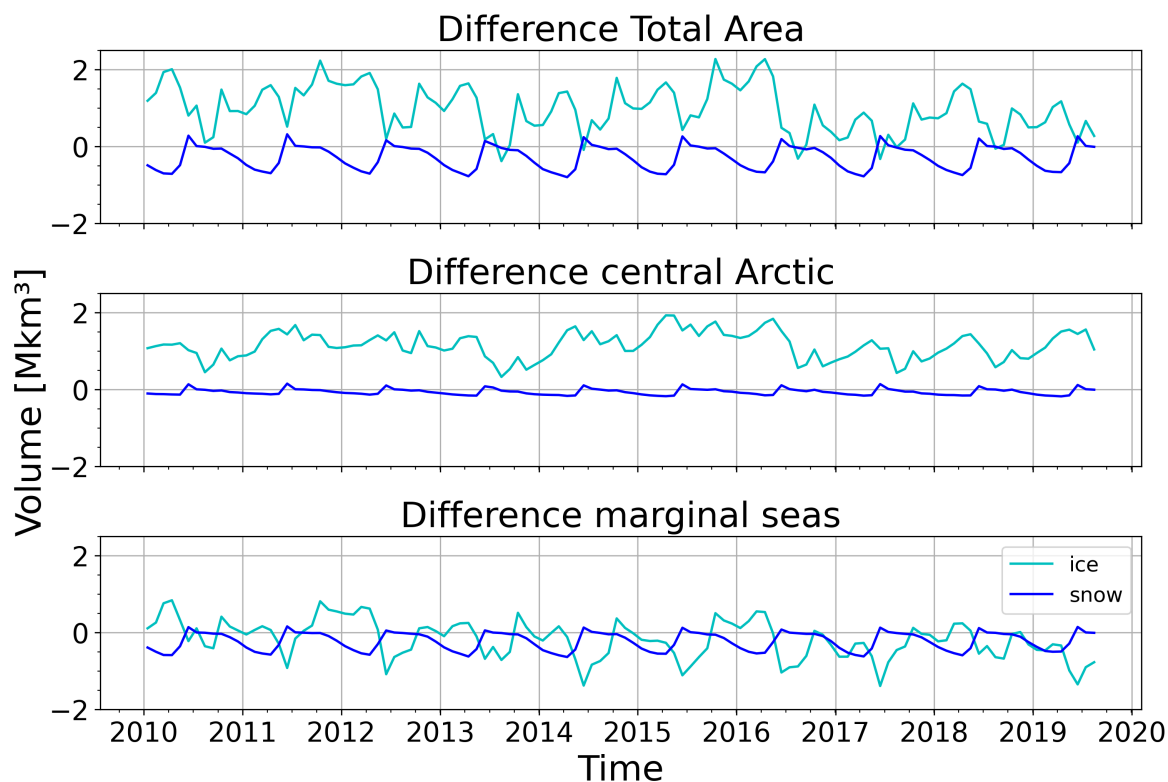
Figure 9. The modelled total sea ice volume difference and snow difference. The turquoise line indicates the ice volume difference calculated as SI3-CICE the blue line snow volume. The upper panel shows the total Arctic ice and snow volume, the middle panel the ice and snow volume difference from thick ice dominated areas (blue mask in figure 1) and the lower panel from thin ice dominated areas (red mask in figure 1).

differences in between the models (Snow blue, Ice turquoise). Both curves display a certain seasonality. Overall, SI3 has a higher sea ice volume than CICE and CICE has a higher snow volume than SI3. The sea ice volume difference peaks each year in the beginning of the freeze-up in September and in the end of the freeze-up in April. The snow volume difference curve has

210 its maximum (higher snow volume in SI3) in June and a minimum (higher snow volume in CICE) in April. The minimum in snow volume difference coincides with the end of freeze-up maximum difference in ice thickness. The correlation between the two volumes differences is -0.5, which means that the snow and ice differences are anticorrelated.

Since the SIT differences in figure 6 left column are differing more in areas covered by thin ice and stays about the same in areas covered by thick multiyear ice (the region north of Greenland and the Canadian Archipelago), the data was divided into

215 thin ice volume and thick ice volume, to be analysed separately. The thin ice areas is indicated by the blue region and the thick ice region by the red region in figure 1. The middle panel in figure 9 shows the snow and ice volume differences for the thick ice covered regions and the lower one the thin ice dominated regions sea ice and snow volume differences.

The thick ice region difference (middle panel figure 9) shows clearly that SI3 has a thicker ice cover in this region overall as found in figure 6. The snow difference is minimal, but there is a clear peak in June (more snow in SI3) as in both other graphs and a slight decrease (towards more snow in CICE) of the snow volume difference throughout the winter season. The sea ice volume also shows a slight seasonality, but by far not as clear as in the upper panel. The correlation was calculated to -0.13. The bottom panel shows the thin ice dominated areas sea ice and snow volume difference. There is a clear seasonality in both sea ice and snow volume difference as already seen in the total area differences in the upper panel. The minimum in sea ice differences (more ice in CICE) occurs each June together with the maximum snow difference (more snow in SI3). The ice volume peaks twice during a year. Once in October and once in April. The peak in April coincides with a minimum in snow volume (more snow in CICE) and the peak in October with the end of the melting season when there is almost no snow in either of the models. The correlation was calculated to -0.56.

3.5 Ice-Ocean and Atmosphere-Ocean drag

The models use different drag formulations to calculate the ocean and atmosphere forcing on sea ice. CICE uses a formulation which computes the drag depending on on SIC, flow size, melt pond, ridges and freeboard, while SI3 uses the same drag coefficient Arctic wide. This drag coefficients are 0.0014 for the atmospheric drag and 0.005 for the ocean drag. Figure 10 shows the difference between CICE and SI3 mean 10 year ocean and atmosphere drag for March and September. In September the atmospheric drag in SI3 is higher in the central Arctic. At the margins and in the coastal regions around Greenland as well as in the Kara Sea CICE drag coefficients exceed SI3s constant value. The September ocean drag is everywhere higher in CICE than in SI3, with maximal values of up to 0.008 in the coastal regions around Greenland and Canada, on the East Siberian shelf and in the Kara and Barents Sea. In March the both the atmosphere and ocean drag in SI3 exceeds CICE drag coefficient in most regions. Only close to the ice edge and close to the coast CICEs drag coefficient is higher than SI3s. The variable ice drag formulation in CICE is higher in the marginal ice zones and the ridged areas north of Greenland and Canada, which means that the ice is more vulnerable to the external forcing.

4 Discussion

Overall, the models compare better to each other than to observations. The models were forced by the same data only the models numerical formulation differ. This links the model observation differences to external forcing and input data and the model differences to the model internal biases.

The differences between the model output and the observational data sets are in good agreement with other model comparison studies. Long et al. (2021) compared NSIDC SIC climatologies from 1979-2014 with the SIC climatologies from all CMIP6 participating models sea ice components. The bias that was found by Long et al. (2021) (figure 1 in Long et al. (2021)) are in many cases bigger than the biases displayed in figure 2. This is expected as the resolution is generally lower within the CMIP6 runs. The models sea ice extent is higher than OSISAF sea ice extent both in March and September. In March the area where the models exceed OSISAF observations at the Atlantic ice edge is over estimated in several ice models (Long et al., 2021) and
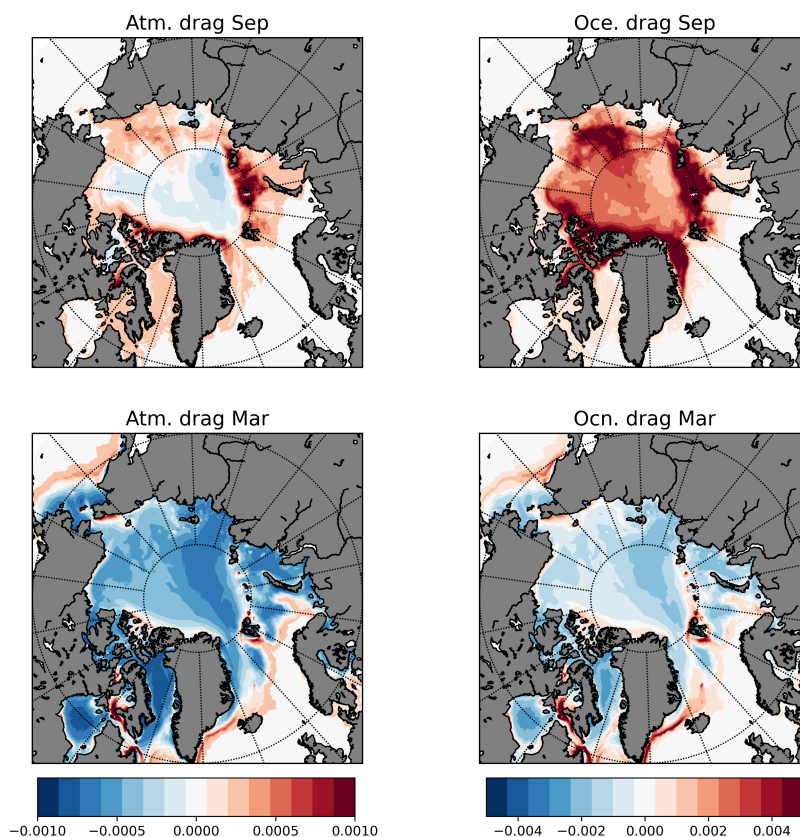
Figure 10. 10 year mean ocean and atmosphere drag difference (CICE-SI3) for March and September.

250   will further be discussed in section 4.1. In summer OSISAF is known to under estimate the ice edge due to melt ponds on ice (Kern et al., 2016). This might lead to some of the September ice edge differences we see in figure 3.

     Comparisons of CS2SMOS data with PIOMAS show similar variability as we find (Wang et al., 2016; Parrinello et al., 2018; Mu et al., 2018a). Mu et al. (2018a) finds that PIOMAS mean SIT in March over a period of 5 years differs by 23cm. Similar calculations for our data sets (averaged over the same region, but over 10 years) show that the SI3 average SIT differs about

255   12cm from CS2SMOS mean March SIT and CICE by only 7cm. This could indicate that the variability and/or trend is smaller in the models compared to PIOMAS. However, PIOMAS should be seen as a point of reference and not the truth as it is also based on a model run, assimilating SIC and sea surface temperature (Zhang and Rothrock, 2003). In general the ice volume from CS2SOMS is not an exact metric either as it also has its uncertainties (Ricker et al., 2017).

     Differences between models and observations were not only found in spacial distribution (figures 2 and 5), but also in the

260   seasonal ice growth as shown in figure 4, which shows the over all sea ice volume per month. The winter growth of CICE and SI3 continues until April, while CS2SMOS sea ice growth slows down in March. Figure 4 also shows that the models over all produce more sea ice than observed. The data shown in figure 4 was masked to only cover the area included in the CS2SMOS

data set. As figure 2 shows the models overestimate the ice edge, which means that there is a significant amount of data not included in figure 4, which is thinner than the included data and melts off first. Hence the apparent sea ice growth from March

265 to April in figure 4 is likely caused by the chosen data points not reflecting the entire ice volume and exclude data point where the models lose ice from March to April. Figure 4 also shows that the models overestimate the total seasonal ice volume growth and melt. Most years the models start into the winter season with less ice than observed and end with more ice than observed. One reason for too much ice loss over the summer season could be the melt of almost all snow in the models. As Figure 7 shows, the Ka/Ku snow product in November has a significant thicker snow layer than SI3 and a slightly thicker snow layer

270 than CICE.

The negative correlation of snow and ice volume differences shown in figure 9 underlines how important the snow layer is for correct sea ice simulation. A large amount of the differences between the models is as figure 9 shows, caused by different treatment of snow, specially in the thin ice region marked blue in figure 1. In the thick ice region the ice-snow difference anticorrelation is with -0.13 significantly lower than the thin ice-snow difference anticorrelation of -0.56. This lower anticor-

275 relation is probably due to the inter-annual variability in the ice differences, which is dominating the variability of the curve. For the snow the main variability still originates from the seasonal cycle. Even though the models are in good agreement with oneanother compared to the differences they show to observations, there are differences between the model. SI3 agrees better with observations in regards to sea ice extent, snow thickness distribution as well as sea ice volume, to a certain extent. CICE performs slightly better according to observations in regards to early winter snow thickness distribution and March sea ice

280 volume.

4.1 Regional differences

In the following section we take a closer look at the differences in the areas (1) Lincoln Sea and Canadian Archipelago, (2) the Atlantic ice edge, (3) Laptev Sea and Siberian shelf, (4) the Chukchi Sea an (5) the Beaufort Sea and where they might originate from. The areas are indicated by their numbers in figure 1. Finally, the parameters, which were found to have the

285 largest effects on the differences in between the models, are discussed.

In area 1, the region north of Greenland and the Canadian Archipelago both models have too little sea ice compared to observations (figure 5) in both March and September. CICE SIT is here about 1 m thinner than SI3 throughout the year (figure 6). CICE agrees better with the CS2SMOS product just off the north coast of Greenland in the Lincoln sea. Moore et al. (2019) Links the sea ice accumulation in region 1 to wind driven ice transport into this region. The sea ice velocities and drag

290 coefficients in winter are lower in CICE than in SI3 (monthly averaged plots of total speed are added in the appendix). This links the difference in drag formulation to the over all thinner ice in CICE compared to SI3. In the Lincoln (region just north off the cost of Greenland) sea SI3 overestimates sea ice, CICE shows realistic values in all seasons. In figure 10 CICE displays a higher drag coefficient in both month and for both atmospheric drag and ocean drag. Tsamados et al. (2015) finds that form drag improves the SIT in this region. Our results agree with this.

295 The overall pattern with larger ice extend in the Barents sea and east of Greenland is known from other models (Long et al., 2021). The overestimation in the Barents sea sea ice extent is according to Li et al. (2017) forced by a lack of oceanic

heat. Since both models show the same pattern in this area and are forced by the same ocean model this is a plausible cause for the model-observation differences. Long et al. (2021) explains the overestimation in East Greenland sea ice extent with the simplicity of the sea-ice model SIS in comparison to CICE. In our study SI3 is the simpler formulated sea-ice model,

300   but performs slightly better than CICE. The general over estimation of the west Greenlandic ice edge is also found in both models which suggests that the formulation of the sea-ice model might not play that big of a role here. Since both models are forced by the same ocean this could hint that the overestimation in this area is also caused by oceanic biases, as mentioned above as a reason for the Barents sea overestimation. The strength of the East Greenlandic current and the front between this and the Atlantic ocean could also cause the bias. This is however only speculation and needs to be investigated further. As

305   mentioned above there is some difference in between CICE and SI3 sea ice extent west of Greenland. As figure 10 shows the drag coefficients of CICEs exceeds the values of SI3. The regions with more SIC in March in figure 3 coincides well with the regions with a significantly higher drag coefficient in CICE located at the ice edge (see figure 10).

SI3 sea ice extent is further north in the Russian shelf region (region 3 in figure 1) than OSISAF and CICE. In the summer month, when little new sea ice is formed SI3 displays stronger north west directed ice velocities (figures in appendix) in this

310   region, which could explain the difference in sea ice extent in between the models. This would also explain the thicker ice during this month in CICE shown in figure 6. Since both models are forced by the same wind fields this difference originates most likely from the difference in drag formulation. Figure 10 shows that the atmospheric drag coefficient in this region are higher in SI3 in September. The ocean drag coefficients are however larger in this region in CICE. Atmospheric circulation is expected to govern the ice drift (Uotila, 2001; Hakkinen et al., 2008), explaining the higher sea ice velocities even though

315   SI3 ocean drag exceeds CICE. The Russian shelf region is shallow and both models calculate grounded ice differently. This could be another reason leading to the differences here. Both modelled SIT in the shelf region differ in lager areas compared to CS2SMOS (Figure 5) than compared to one another. Watts et al. (2021) finds that the ocean heat transport could be the reason that grows and melt is not properly resolved in most models. The remaining difference between the models could be explained by differing formulations for grounded and land fast ice.

320   In March SI3 has up to a meter more ice in the Chukchi sea (region 4 in figure 1) than CICE. Comparing the models to the CS2SMOS product CICE agrees better with observations than SI3 in this region. Petty et al. (2016) describe how a faster spinning Beaufort gyre accumulates more ice in the Chukchi Sea. Comparing average sea ice velocities in the Beaufort Sea shows that SI3 sea ice velocities (figures in appendix) in this region are higher than CICEs in most month. CICE drag coefficients in March (lower row in figure 10) are also higher than SI3s. Since both models are force by the same ocean and

325   atmosphere data this is a strong evidence that the difference in drag formulation in the models lead to thicker ice in the Chukchi Sea in SI3.

In the Beaufort Sea CICEs SIT is over all thinner than SI3s. Both models have thicker sea ice in the Beaufort Sea (region 5 in figure 1) than observed (figure 4), with a better agreement between CICE and CS2SMOS. The mean sea ice velocities in the Beaufort gyre are during all month higher in SI3 than in CICE. The drag coefficients in figure 10 however are only higher SI3

330   in March. The resulting higher sea ice velocities in summer are most likely resulting from the lower SIC in SI3 (3). The SIC differences in summer are most likely caused by the albedo differences. The spin of the Beaufort gyre highly depends on the

sea ice motion forced by winds. This relation is known as the Ice-Ocean Governor (Meneghello et al., 2018) and is known to control the sea surface height in the Beaufort sea. In our results, a faster spinning ice field in the Beaufort Sea also leads to a thicker sea ice cover. How this influences the underlying ocean out of the scope of this study.

Overall the drag coefficient plays an important role in the differences in between the models. In many region (Lincoln Sea, Russian shelf area, Chukchi Sea and Beaufort Sea) the from drag formulation most likely leads to a model result closer to the observations. Over all CICE, which is the model using the formdrag has a thinner ice layer than SI3 which as Castellani et al. (2018) points out might be caused by the form drag. Comparing the albedo values of the two models shows that CICE calculates in general lower albedo values in summer than SI3. This is most likely an other reason for the generally lower sea ice volume in CICE.

Another reason for the lower sea ice volume in CICE is the different treatment of snow. Especially in late winter, the overall snow cover is thinner in SI3 than in CICE (figure 7, 9, 8). Figure 7 shows how the snow grows faster and thicker over the winter month in CICE than in SI3. The blue curve in figure 9 shows that CICE total snow volume in March exceeds SI3 snow volume by about 0.8 Mkm^2. The March snow climatology in figure 8 shows the special distribution of the differences. SI3 agrees better with observations in the last month as figure 7 shows. SI3s snow scheme included a reduction of the snow cover due to blowing snow and ridging and rafting. In the presented set up this means that the snow over ridges and rafts is reduced by 50% and a blowing snow parameter of 0.66 for a blowing snow parametrisation following Ledley (1985). Over all this parametrisation leads to a better agreement with observations.

5 Conclusions

We compared the sea-ice models CICE and SI3 under equal forcing, grid set up and coupled to the same ocean model. By this we aim to get a better understanding of how much variability is cased by the choice of sea-ice models and identify model processes that drive differences in resulting sea ice predictions, which could help better interpret there results in general. This study also presents a new sea ice ocean model set up with NEMO4 coupled to the sea-ice model CICE version 6.2. The results show that the set up performs comparable to other sea-ice models.

Overall the models compare well to observations and their differences are in a range similar to other model comparisons (Wang et al., 2016; Parrinello et al., 2018; Mu et al., 2018a; Long et al., 2021). The biggest differences between the models were found in the total sea ice volume. SI3 produces thicker sea ice than CICE. CICE on the other hand shows a larger sea ice extent in any season. OSISAF sea ice observations agree better with SI3. Both models differ significantly from CR2SOMS SIT retrievals and produce more ice throughout the winter season. Both models differ in snow thickness from observations and from each other. The differences in between the models are not as significant as the difference both models show in respect to the Ka/Ku snow product.

Several processes could be link to the discussed model differences. These are the drag formulation, the albedo calculation and the treatment of snow. The formdrag formulation in CICE results in better sea ice simulations locally in the Chukchi sea, Beaufort Sea as well as in the Russian shelf region, but might cause an overestimation of the ice edge and an overall thinner SIT

365   as also found by Castellani et al. (2018). The tuning in this study was done by comparing models total Arctic sea ice volume
       to PIOMAS (Schweiger et al., 2011b) total sea ice volume. The resulting albedo differs significantly with SI3 reflecting a large
       amount of the short wave radiation, which was linked to the overall thicker sea ice cover. The tuning in the models was done
       manually testing varying each of the albedo parameters one by one and comparing the result to total sea ice volume. With the
       snow and ice layer changing through out the seasons and several parameters at play which have different effect in different
370   regions depending on the season it would be advisable to use a more sophisticated tuning method as for example Panteleev
       et al. (2020) or Massonnet et al. (2014).

       The third and most significant differences is resulting from different treatment of snow. Both models are forced by the same
       atmospheric forcing what means that the same amount of snow arrives at the ice surface. As figure 9 shows the development
       of the snow through out the year is significantly different and correlates negatively with the differences in SIT especially over
375   newly formed ice. The negative correlation in between the differences is significant and differences in both SIT and SIC in the
       models output can be linked to the snow thickness differences. The comparison to the Ka/Ku snow thickness observations shows
       that the snow thickness is differing more from observations than from each other. Our results show that better representation
       of the snow layer in models will also improve the sea ice prediction.

       Data availability. sea-ice model output data can be provided upon request.

380   **Appendix A: Sea Ice velocity**
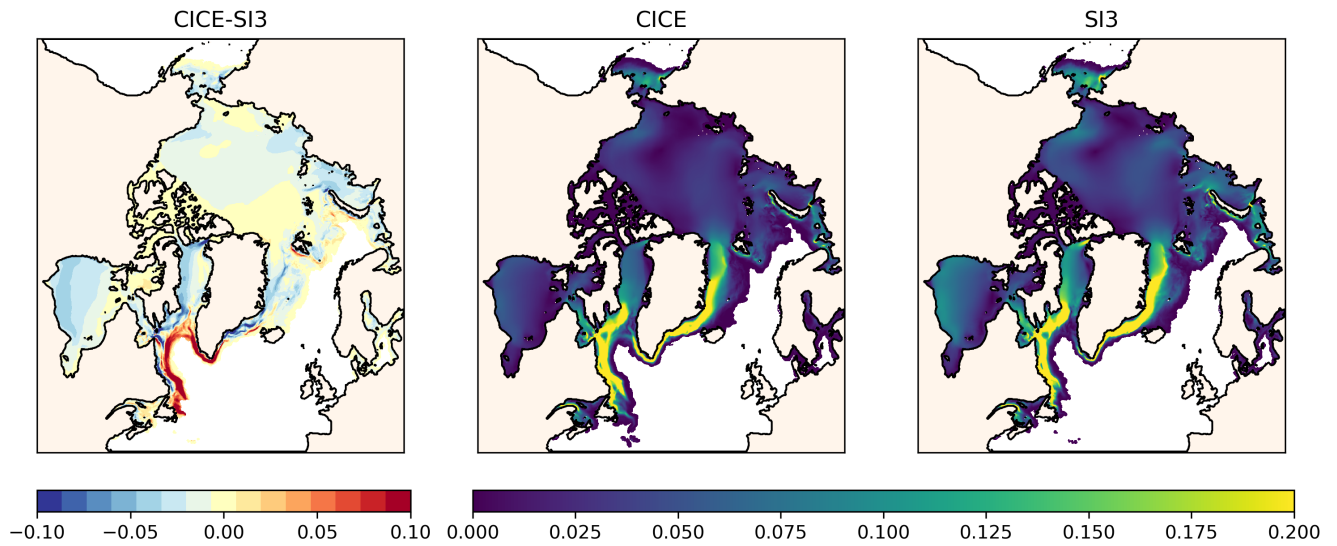
Figure A1. 10 year mean sea ice velocities for January from model output. Left panel: CICE-SI3 differences, middle panel: CICE total velocities, right panel: SI3 total velocities.
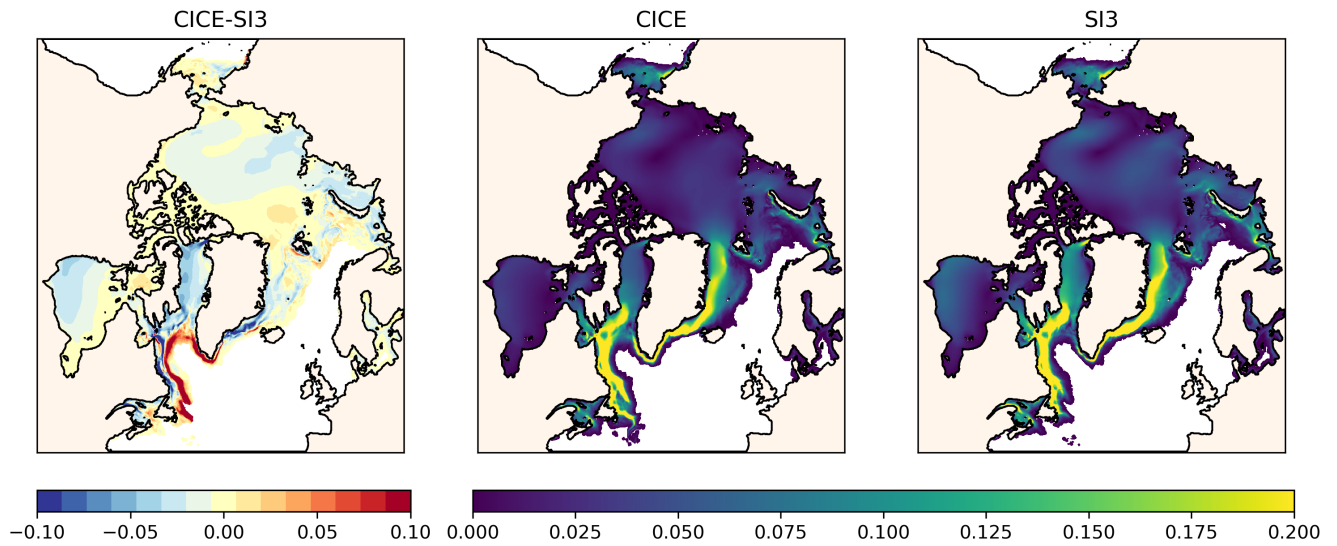
Figure A2. 10 year mean sea ice velocities for February from model output. Left panel: CICE-SI3 differences, middle panel: CICE total velocities, right panel: SI3 total velocities.
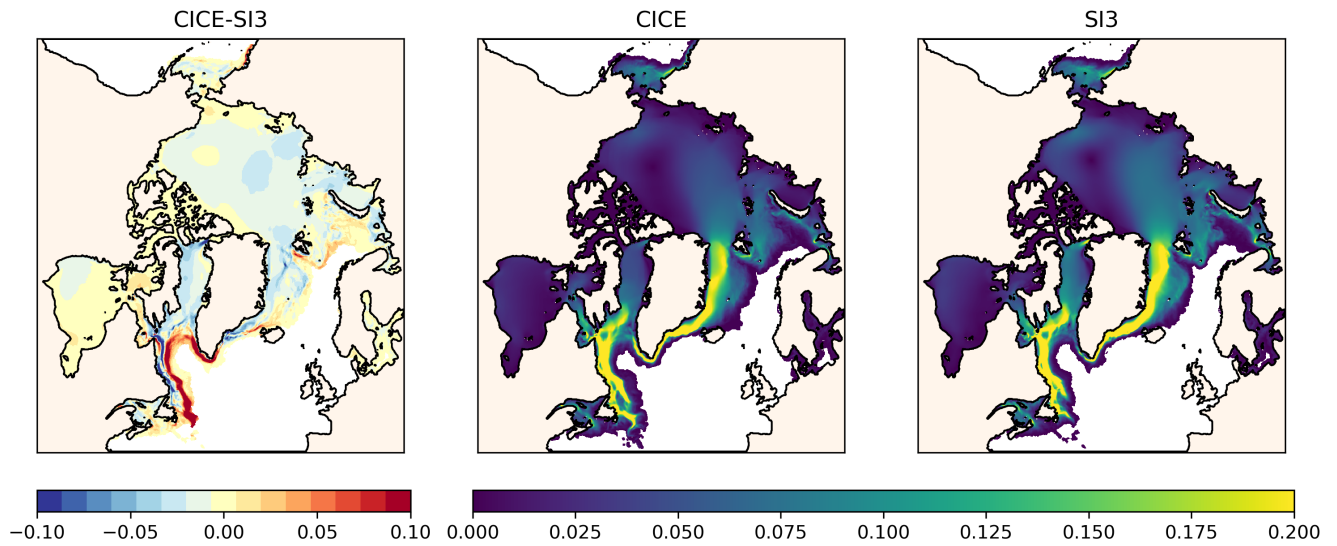
Figure A3. 10 year mean sea ice velocities for March from model output. Left panel: CICE-SI3 differences, middle panel: CICE total velocities, right panel: SI3 total velocities.
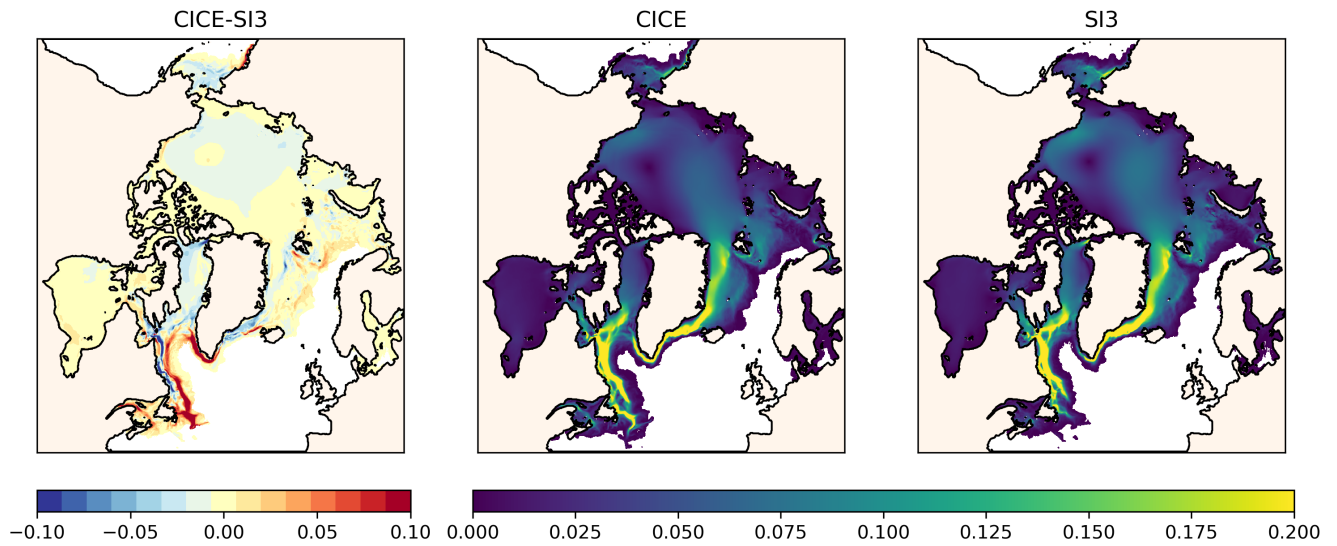
Figure A4. 10 year mean sea ice velocities for April from model output. Left panel: CICE-SI3 differences, middle panel: CICE total velocities, right panel: SI3 total velocities.
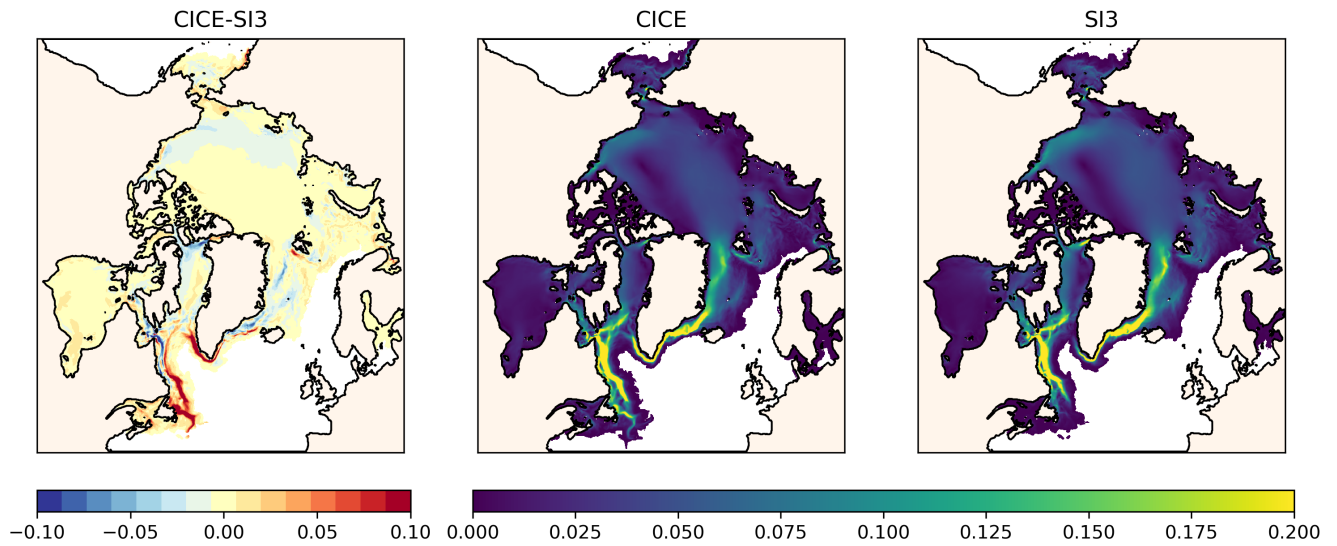
Figure A5. 10 year mean sea ice velocities for May from model output. Left panel: CICE-SI3 differences, middle panel: CICE total velocities, right panel: SI3 total velocities.
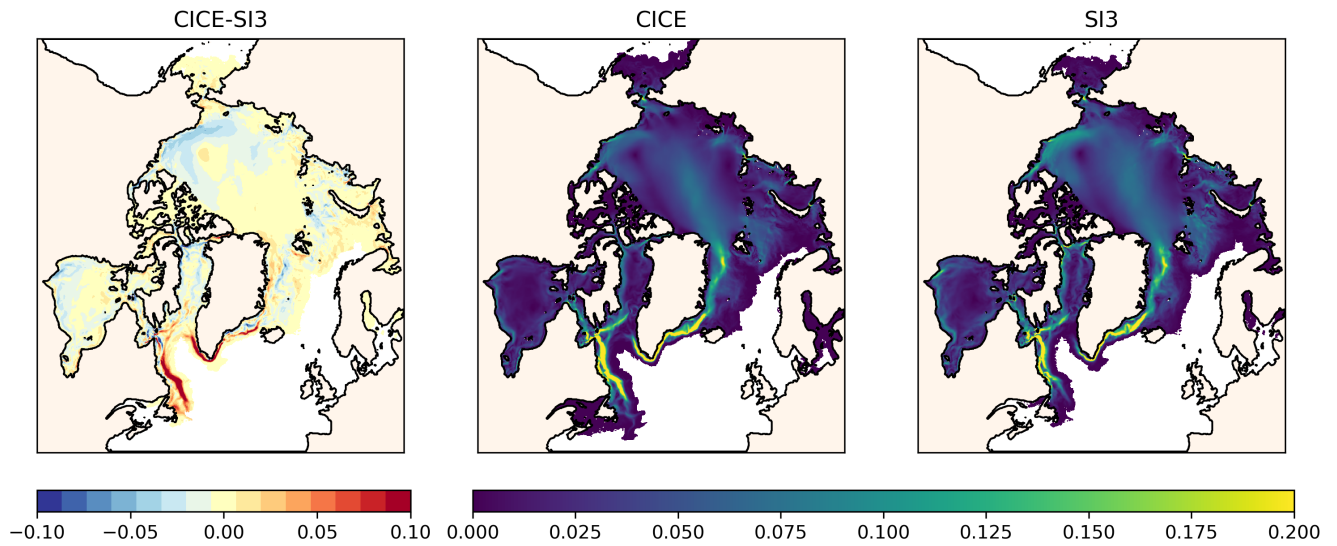
Figure A6. 10 year mean sea ice velocities for June from model output. Left panel: CICE-SI3 differences, middle panel: CICE total velocities, right panel: SI3 total velocities.
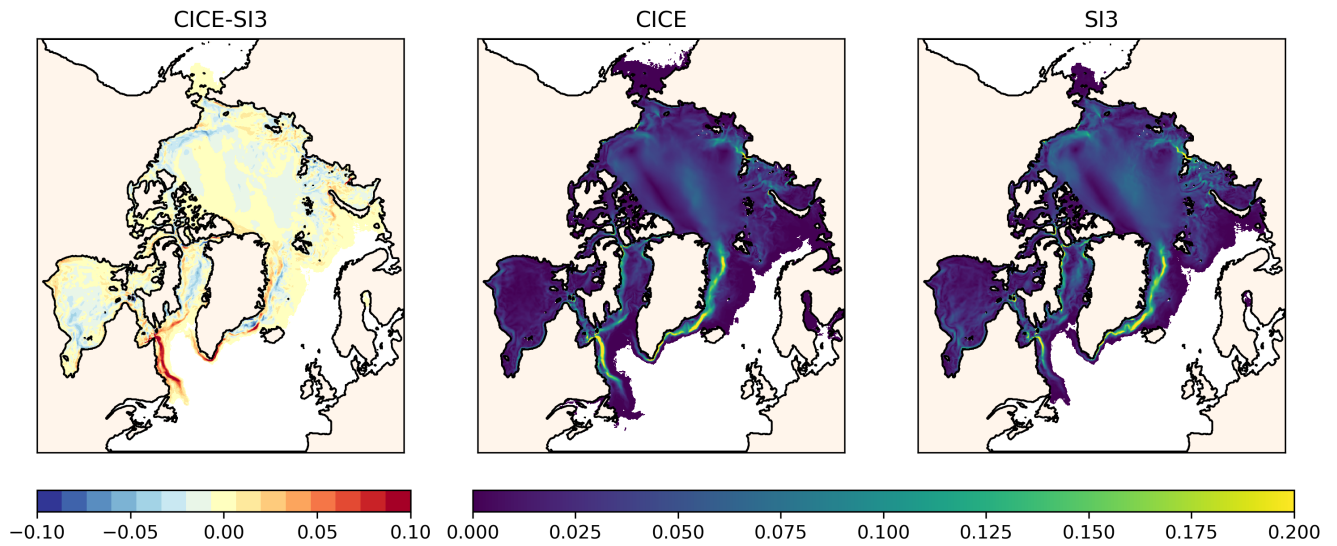
Figure A7. 10 year mean sea ice velocities for July from model output. Left panel: CICE-SI3 differences, middle panel: CICE total velocities, right panel: SI3 total velocities.
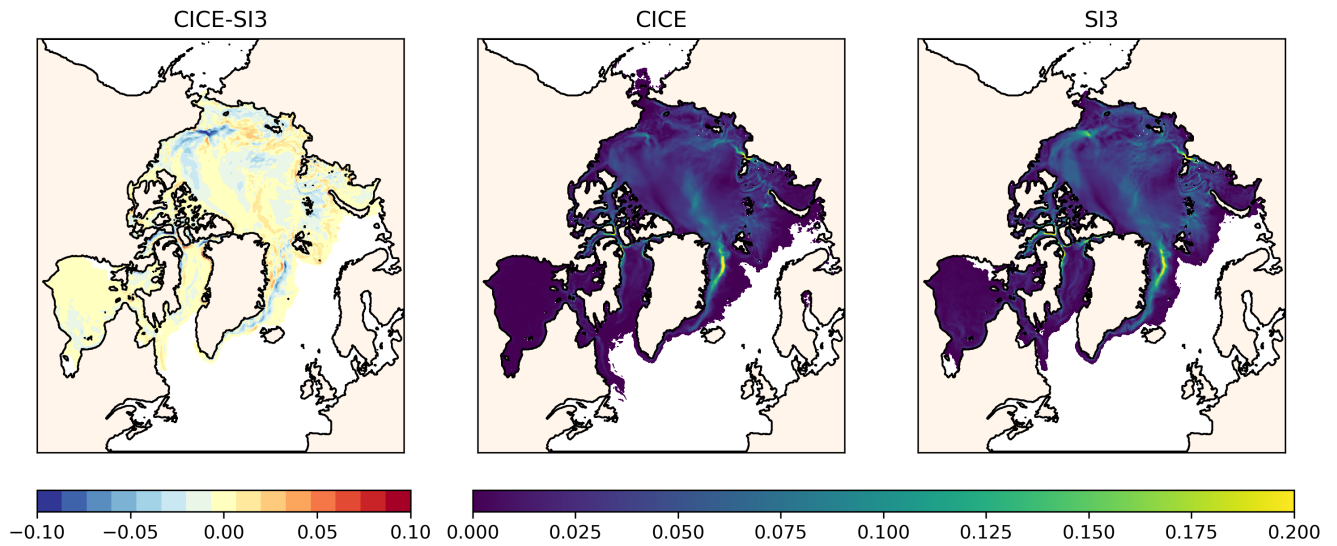
Figure A8. 10 year mean sea ice velocities for August from model output. Left panel: CICE-SI3 differences, middle panel: CICE total velocities, right panel: SI3 total velocities.
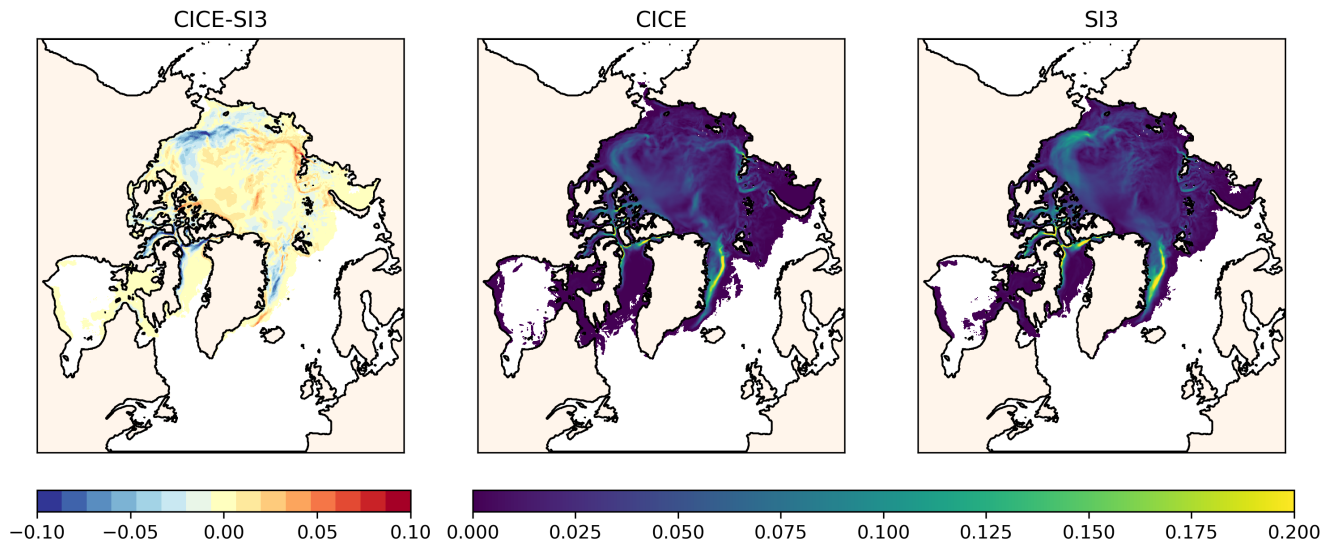
Figure A9. 10 year mean sea ice velocities for September from model output. Left panel: CICE-SI3 differences, middle panel: CICE total velocities, right panel: SI3 total velocities.
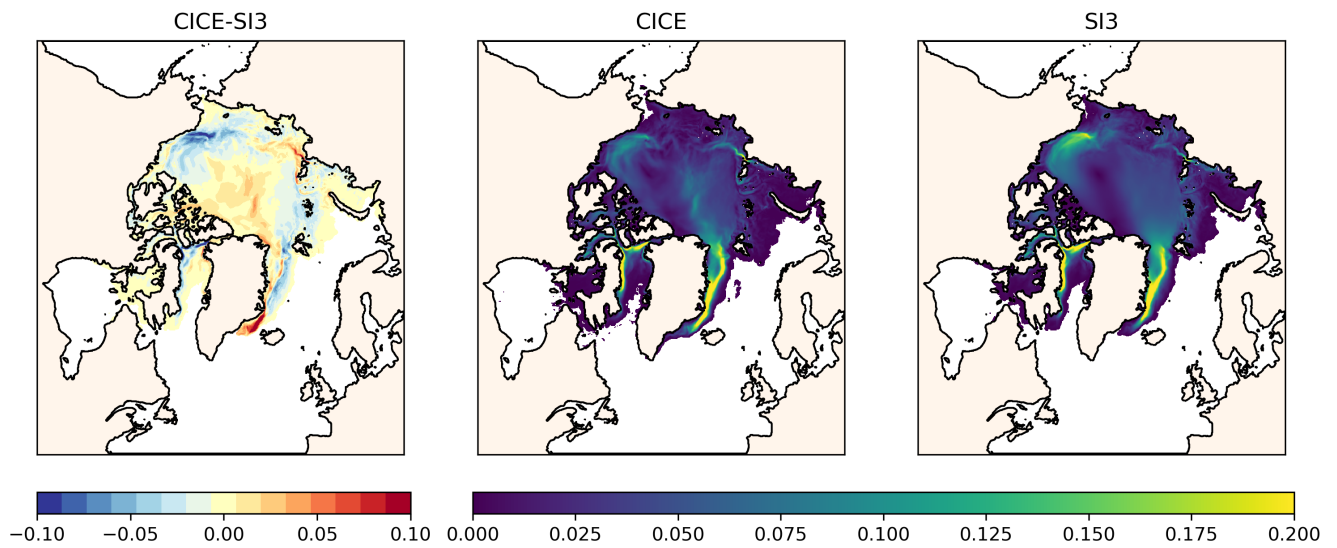
Figure A10. 10 year mean sea ice velocities for October from model output. Left panel: CICE-SI3 differences, middle panel: CICE total velocities, right panel: SI3 total velocities.
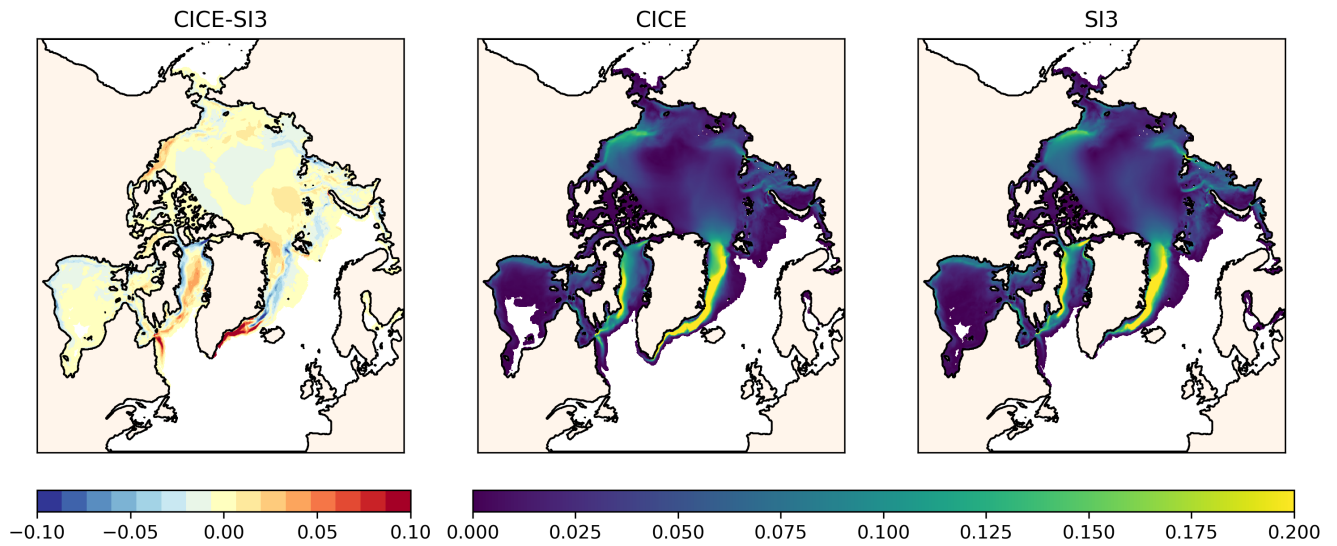
Figure A11. 10 year mean sea ice velocities for November from model output. Left panel: CICE-SI3 differences, middle panel: CICE total velocities, right panel: SI3 total velocities.
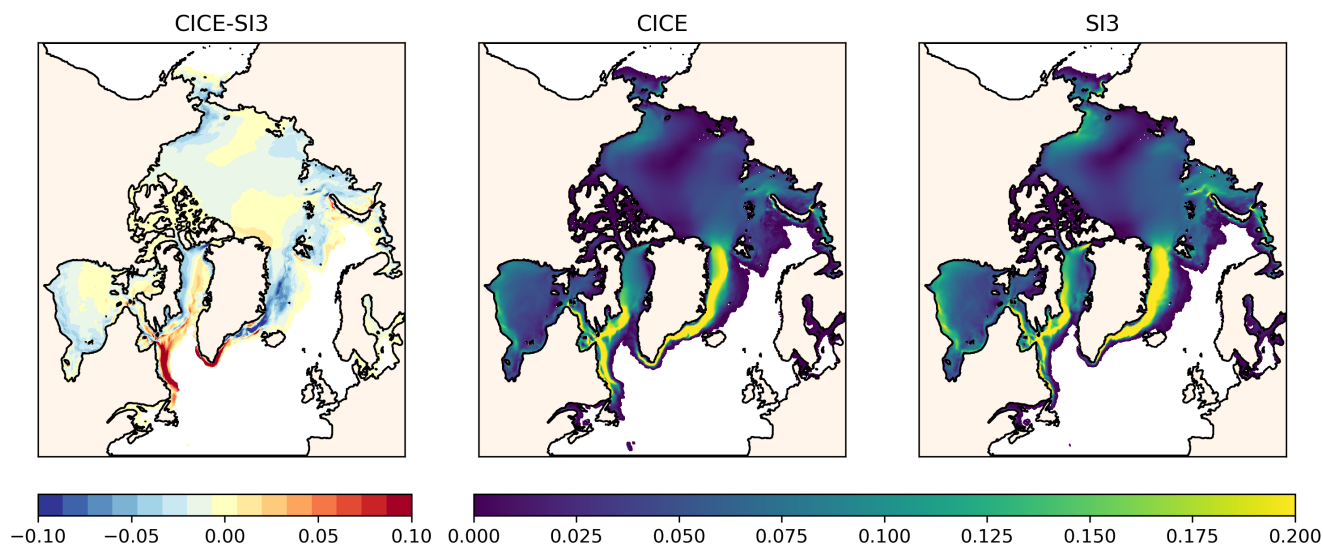
Figure A12. 10 year mean sea ice velocities for December from model output. Left panel: CICE-SI3 differences, middle panel: CICE total velocities, right panel: SI3 total velocities.

Author contributions. IS ran the CICE model experiment, wrote the manuscript draft and analysed the model output, ANG ran the SI3 model experiment, ANG and TAR, contributed to the introduction and method section of the manuscript, RH set up of the ocean model, ANG, TAR, RH and LS edited and reviewed the manuscript.

Competing interests. To the knowledge of the authors there are no competing interest

385 *Acknowledgements.* This study is a collaboration between the Danish Meteorological Institute, Aalborg University and the Danish Technical University. It is funded by the Danish State through the National centre for Climate Research.

The model input contains Copernicus Climate Change Service information (2021) and neither the European Commission nor ECMWF is responsible for any use that may be made of the Copernicus information or data it contains.

References

390   Blanchard-Wrigglesworth, E., Farrell, S. L., Newman, T., and Bitz, C. M.: Snow cover on Arctic sea ice in observations and an Earth System
Model, Geophysical Research Letters, 42, 10,342–10,348, https://doi.org/https://doi.org/10.1002/2015GL066049, 2015.

Briegleb, B. and Light, B.: A Delta-Eddington multiple scattering parameterization for solar radiation in the sea ice component of the
Community Climate System Model, NCAR technical note, pp. 1–108, 2007.

Castellani, G., Losch, M., Ungermann, M., and Gerdes, R.: Sea-ice drag as a function of deformation and ice cover: Effects on simulated sea
395   ice and ocean circulation in the Arctic, Ocean Modelling, 128, 48–66, 2018.

Collow, T. W., Wang, W., Kumar, A., and Zhang, J.: Improving Arctic Sea Ice Prediction Using PIOMAS Initial Sea Ice Thickness in a
Coupled Ocean–Atmosphere Model, Monthly Weather Review, 143, 4618 – 4630, https://doi.org/10.1175/MWR-D-15-0097.1, 2015.

Dai, A. and Trenberth, K. E.: Estimates of freshwater discharge from continents: Latitudinal and seasonal variations, Journal of hydromete-
orology, 3, 660–687, 2002.

400   Day, J., Hawkins, E., and Tietsche, S.: Will Arctic sea ice thickness initialization improve seasonal forecast skill?, Geophysical Research
Letters, 41, 7566–7575, 2014.

Dirkson, A., Merryfield, W. J., and Monahan, A.: Impacts of sea ice thickness initialization on seasonal Arctic sea ice predictions, Journal of
Climate, 30, 1001–1017, 2017.

Dupont, F., Higginson, S., Bourdallé-Badie, R., Lu, Y., Roy, F., Smith, G. C., Lemieux, J.-F., Garric, G., and Davidson, F.: A high-resolution
405   ocean and sea-ice modelling system for the Arctic and North Atlantic oceans, Geoscientific Model Development, 8, 1577–1594, 2015.

Egbert, G. D. and Erofeeva, S. Y.: Efficient inverse modeling of barotropic ocean tides, Journal of Atmospheric and Oceanic technology, 19,
183–204, 2002.

Garnier, F., Fleury, S., Garric, G., Bouffard, J., Tsamados, M., Laforge, A., Bocquet, M., Fredensborg Hansen, R. M., and Rémy, F.: Advances
in altimetric snow depth estimates using bi-frequency SARAL/CryoSat-2 Ka/Ku measurements, The Cryosphere Discussions, 2021, 1–40,
410   https://doi.org/10.5194/tc-2021-79, 2021.

Hakkinen, S., Proshutinsky, A., and Ashik, I.: Sea ice drift in the Arctic since the 1950s, Geophysical Research Letters, 35, 2008.

Hazeleger, W., Wang, X., Severijns, C., Ştefănescu, S., Bintanja, R., Sterl, A., Wyser, K., Semmler, T., Yang, S., Van den Hurk, B., et al.:
EC-Earth V2. 2: description and validation of a new seamless earth system prediction model, Climate dynamics, 39, 2611–2629, 2012.

Hersbach, H., Bell, B., Berrisford, P., Hirahara, S., Horányi, A., Muñoz Sabater, J., Nicolas, J., Peubey, C., Radu, R., Schepers, D., Simmons,
415   A., Soci, C., Abdalla, S., Abellan, X., Balsamo, G., Bechtold, P., Biavati, G., Bidlot, J., Bonavita, M., De Chiara, G., Dahlgren, P., Dee,
D., Diamantakis, M., Dragani, R., Flemming, J., Forbes, R., Fuentes, M., Geer, A., Haimberger, L., Healy, S., Hogan, R. J., Hólm, E.,
Janisková, M., Keeley, S., Laloyaux, P., Lopez, P., Lupu, C., Radnoti, G., de Rosnay, P., Rozum, I., Vamborg, F., Villaume, S., and Thépaut,
J.-N.: Complete ERA5: Fifth generation of ECMWF atmospheric reanalyses of the global climate, Copernicus Climate Change Service
(C3S) Data Store (CDS), accessed in 2021, 2017.

420   Hordoir, R., Axell, L., Höglund, A., Dieterich, C., Fransner, F., Gröger, M., Liu, Y., Pemberton, P., Schimanke, S., Andersson, H., Ljungemyr,
P., Nygren, P., Falahat, S., Nord, A., Jönsson, A., Lake, I., Döös, K., Hieronymus, M., Dietze, H., Löptien, U., Kuznetsov, I., Westerlund,
A., Tuomi, L., and Haapala, J.: Nemo-Nordic 1.0: a NEMO-based ocean model for the Baltic and North seas – research and operational
applications, Geoscientific Model Development, 12, 363–386, https://doi.org/10.5194/gmd-12-363-2019, 2019.

Hordoir, R., Skagseth, Ø., Ingvaldsen, R. B., Sandø, A. B., Löptien, U., Dietze, H., Gierisch, A. M., Assmann, K. M., Lundesgaard, Ø., and
    Lind, S.: Changes in Arctic Stratification and Mixed Layer Depth Cycle: A Modeling Analysis, Journal of Geophysical Research: Oceans,
    127, e2021JC017 270, 2022.

Hunke, E., Allard, R., Bailey, D. A., Blain, P., Craig, A., Dupont, F., DuVivier, A., Grumbine, R., Hebert, D., Holland, M., Jeffery, N.,
    Lemieux, J.-F., Osinski, R., Rasmussen, T., Ribergaard, M., Roberts, A., Turner, M., Winton, M., and Rethmeier, S.: CICE Version 6.2.0,
    https://github.com/CICE-Consortium/CICE/tree/CICE6.2.0, 2021a.

Hunke, E., Allard, R., Bailey, D. A., Blain, P., Craig, A., Dupont, F., DuVivier, A., Grumbine, R., Hebert, D., Holland, M., Jeffery,
    N., Lemieux, J.-F., Osinski, R., Rasmussen, T., Ribergaard, M., Roberts, A., Turner, M., Winton, M., and Rethmeier, S.: CICE-
    Consortium/CICE: CICE Version 6.2.0, https://doi.org/10.5281/zenodo.4671172, 2021b.

Kacimi, S. and Kwok, R.: Arctic snow depth, ice thickness and volume from ICESat-2 and CryoSat-2: 2018-2021, Geophysical Research
    Letters, p. e2021GL097448, 2022.

Kashiwase, H., Ohshima, K. I., Nihashi, S., and Eicken, H.: Evidence for ice-ocean albedo feedback in the Arctic Ocean shifting to a seasonal
    ice zone, Scientific Reports, 8170, https://doi.org/10.1038/s41598-017-08467-z, 2017.

Kern, S., Rösel, A., Pedersen, L. T., Ivanova, N., Saldo, R., and Tonboe, R. T.: The impact of melt ponds on summertime microwave
    brightness temperatures and sea-ice concentrations, The Cryosphere, 10, 2217–2239, 2016.

Kiss, A. E., Hogg, A. M., Hannah, N., Boeira Dias, F., Brassington, G. B., Chamberlain, M. A., Chapman, C., Dobrohotoff, P., Domingues,
    C. M., Duran, E. R., et al.: ACCESS-OM2 v1. 0: a global ocean–sea ice model at three resolutions, Geoscientific Model Development,
    13, 401–442, 2020.

Le Sommer, J., Molines, J., Albert, A., Brodeau, L., Ajayi, A., Gomez Navarro, L., Cosme, E., Penduff, T., Barnier, B., Verron, J., et al.:
    NATL60: A North Atlantic ocean circulation model dataset based on NEMO for preparing SWOT altimeter mission, in prep, preparation
    for Geoscientific Model Development, 2019.

Ledley, T. S.: Sensitivity of a thermodynamic sea ice model with leads to time step size, Journal of Geophysical Research: Atmospheres, 90,
    2251–2260, 1985.

Lellouche, J.-M., Greiner, E., Bourdallé-Badie, R., Garric, G., Melet, A., Drévillon, M., Bricaud, C., Hamon, M., Le Galloudec, O., Regnier,
    C., et al.: The Copernicus global 1/12° oceanic and sea ice GLORYS12 reanalysis, Frontiers in Earth Science, 9, 585, 2021.

Li, D., Zhang, R., and Knutson, T. R.: On the discrepancy between observed and CMIP5 multi-model simulated Barents Sea winter sea ice
    decline, Nature Communications, 8, 1–7, 2017.

Long, M., Zhang, L., Hu, S., and Qian, S.: Multi-Aspect Assessment of CMIP6 Models for Arctic Sea Ice Simulation, Journal of Climate,
    34, 1515–1529, 2021.

Losch, M., Menemenlis, D., Campin, J.-M., Heimbach, P., and Hill, C.: On the formulation of sea-ice mod-
    els. Part 1: Effects of different solver implementations and parameterizations, Ocean Modelling, 33, 129–144,
    https://doi.org/https://doi.org/10.1016/j.ocemod.2009.12.008, 2010.

Madec, G., Bourdallé-Badie, R., Bouttier, P.-A., Bricaud, C., Bruciaferri, D., Calvert, D., Chanut, J., Clementi, E., Coward, A., Delrosso, D.,
    et al.: NEMO ocean engine, 2017.

Massonnet, F., Goosse, H., Fichefet, T., and Counillon, F.: Calibration of sea ice dynamic parameters in an ocean-sea ice model using an
    ensemble Kalman filter, Journal of Geophysical Research: Oceans, 119, 4168–4184, 2014.

Meneghello, G., Marshall, J., Campin, J.-M., Doddridge, E., and Timmermans, M.-L.: The ice-ocean governor: Ice-ocean stress feedback
    limits Beaufort Gyre spin-up, Geophysical Research Letters, 45, 11–293, 2018.

Moore, G., Schweiger, A., Zhang, J., and Steele, M.: Spatiotemporal variability of sea ice in the arctic's last ice area, Geophysical Research Letters, 46, 11 237–11 243, 2019.

Mu, L., Losch, M., Yang, Q., Ricker, R., Losa, S. N., and Nerger, L.: Arctic-wide sea ice thickness estimates from combining satellite remote sensing data and a dynamic ice-ocean model with data assimilation during the CryoSat-2 period, Journal of Geophysical Research: Oceans, 123, 7763–7780, 2018a.

Mu, L., Yang, Q., Losch, M., Losa, S. N., Ricker, R., Nerger, L., and Liang, X.: Improving sea ice thickness estimates by assimilating CryoSat-2 and SMOS sea ice thickness data simultaneously, Quarterly Journal of the Royal Meteorological Society, 144, 529–538, 2018b.

NEMO-Sea-Ice-Working-Group: Sea Ice modelling Integrated Initiative (SI^3) – The NEMO sea ice engine, https://doi.org/10.5281/zenodo.1471689, 2022.

OSISAF: Global Sea Ice Concentration Climate Data Record v2. 0–Multimission, EUMETSAT SAF on Ocean and Sea Ice, 2017.

Panteleev, G., Yaremchuk, M., Stroh, J. N., Francis, O. P., and Allard, R.: Parameter optimization in sea ice models with elastic–viscoplastic rheology, The Cryosphere, 14, 4427–4451, 2020.

Parrinello, T., Shepherd, A., Bouffard, J., Badessi, S., Casal, T., Davidson, M., Fornari, M., Maestroni, E., and Scagliola, M.: CryoSat: ESA's ice mission–Eight years in space, Advances in Space Research, 62, 1178–1190, 2018.

Petty, A. A., Hutchings, J. K., Richter-Menge, J. A., and Tschudi, M. A.: Sea ice circulation around the Beaufort Gyre: The changing role of wind forcing and the sea ice state, Journal of Geophysical Research: Oceans, 121, 3278–3296, 2016.

Ricker, R., Hendricks, S., Kaleschke, L., Tian-Kunze, X., King, J., and Haas, C.: A weekly Arctic sea-ice thickness data record from merged CryoSat-2 and SMOS satellite data, The Cryosphere, 11, 1607–1623, https://doi.org/10.5194/tc-11-1607-2017, 2017.

Schweiger, A., Lindsay, R., Zhang, J., Steele, M., Stern, H., and Kwok, R.: Uncertainty in modeled Arctic sea ice volume, Journal of Geophysical Research: Oceans, 116, 2011a.

Schweiger, A., Lindsay, R., Zhang, J., Steele, M., Stern, H., and Kwok, R.: Uncertainty in modeled Arctic sea ice volume, Journal of Geophysical Research: Oceans, 116, 2011b.

Shine, K. and Henderson-Sellers, A.: The sensitivity of a thermodynamic sea ice model to changes in surface albedo parameterization, Journal of Geophysical Research: Atmospheres, 90, 2243–2250, 1985.

Smith, G. C., Liu, Y., Benkiran, M., Chikhar, K., Surcel Colan, D., Gauthier, A.-A., Testut, C.-E., Dupont, F., Lei, J., Roy, F., et al.: The Regional Ice Ocean Prediction System v2: a pan-Canadian ocean analysis system using an online tidal harmonic analysis, Geoscientific Model Development, 14, 1445–1467, 2021.

Stewart, E. J., Liggett, D., Lamers, M., Ljubicic, G., Dawson, J., Thoman, R., Haavisto, R., and Carrasco, J.: Characterizing polar mobilities,to understand the role of weather, water, ice and climate (WWIC) information, Polar Geography, 43, https://doi.org/10.1080/1088937X.2019.1707319, 2020.

Stocker, A. N., Renner, A. H., and Knol-Kauffman, M.: Sea ice variability and maritime activity around Svalbard in the period 2012–2019, Scientific reports, 10, 1–12, 2020.

Tonboe, R. T., Eastwood, S., Lavergne, T., Sørensen, A. M., Rathmann, N., Dybkjær, G., Pedersen, L. T., Høyer, J. L., and Kern, S.: The EUMETSAT sea ice concentration climate data record, The Cryosphere, 10, 2275–2290, https://doi.org/10.5194/tc-10-2275-2016, 2016.

Tsamados, M., Feltham, D., Petty, A., Schroeder, D., and Flocco, D.: Processes controlling surface, bottom and lateral melt of Arctic sea ice in a state of the art sea ice model, Philosophical Transactions of the Royal Society A: Mathematical, Physical and Engineering Sciences, 373, 20140 167, 2015.

Uotila, J.: Observed and modelled sea-ice drift response to wind forcing in the northern Baltic Sea, Tellus A, 53, 112–128, 2001.

500   Wagner, P. M., Hughes, N., Bourbonnais, P., Stroeve, J., Rabenstein, L., Bhatt, U., Little, J., Wiggins, H., and Fleming, A.: Sea-ice information and forecast needs for industry maritime stakeholders, Polar Geography, 43, 160–187, https://doi.org/10.1080/1088937X.2020.1766592, 2020.

Wang, C., Graham, R. M., Wang, K., Gerland, S., and Granskog, M. A.: Comparison of ERA5 and ERA-Interim near surface air temperature and precipitation over Arctic sea ice: Effects on sea ice thermodynamics and evolution, in: AGU Fall Meeting Abstracts, vol. 2018, pp.
505   C33F–1626, 2018.

Wang, X., Key, J., Kwok, R., and Zhang, J.: Comparison of Arctic sea ice thickness from satellites, aircraft, and PIOMAS data, Remote Sensing, 8, 713, 2016.

Watts, M., Maslowski, W., Lee, Y. J., Kinney, J. C., and Osinski, R.: A spatial evaluation of Arctic sea ice and regional limitations in CMIP6 historical simulations, Journal of Climate, 34, 6399–6420, 2021.

510   Zhang, J. and Rothrock, D. A.: Modeling global sea ice with a thickness and enthalpy distribution model in generalized curvilinear coordinates, Monthly Weather Review, 131, 845–861, 2003.

Zuo, H., Balmaseda, M. A., Tietsche, S., Mogensen, K., and Mayer, M.: The ECMWF operational ensemble reanalysis–analysis system for ocean and sea ice: a description of the system and assessment, Ocean science, 15, 779–808, 2019.